A Lens Antenna Array With Adaptive Optical Processing

Edeline Fotheringham, Stefania Römisch, Paul C. Smith, Darko Popovic, Dana Z. Anderson, and Zoya Popovic, *Fellow, IEEE*

***Abstract*—This paper presents an *X* band smart antenna array in which adaptive processing of the received signals is performed by dynamic holographic optical circuitry. The optical circuitry adaptively extracts the principal component of the received signal space, that is the strongest first-order independent temporal component of the ensemble of received signals. The adaptive receiver system can be used, for example, to mitigate multipath interference effects and can separate one received signal from another even though their power spectra may entirely overlap. A prototype two-channel system is designed to fit in a standard-size briefcase and consume less than 50 W of power. The input to the system are modulated waves with a carrier in *X* band and the output is an electronic demodulated signal. Three major components of this system are described in detail: 1) the quasi-optical lens antenna array front end with angle-of-arrival preprocessing and downconversion, 2) the two-channel electrooptic modulation and optical carrier suppression stage, and 3) the smart optical processor (auto-tuning filter). Component and end-to-end system measurements give quantitative indicators for the usefulness of optical processing in wireless communications.**

***Index Terms*—Adaptive antenna arrays, nonlinear optics, photorefractive effect.**

I. Introduction

THIS paper presents an *X* band smart antenna array in which adaptive processing of the received signals is performed by dynamic holographic optical circuitry. The optical circuitry adaptively extracts the principal component of the received signal space [1], that is, the strongest first-order independent temporal component of the ensemble of received signals. The adaptive receiver system can be used, for example, to mitigate multipath interference effects and can separate one received signal from another even though their power spectra may entirely overlap. This work is intended to illustrate the use of nonlinear optical techniques that can simplify smart antenna systems [2] and partially relieve the computational burden placed on digital signal processing. We have designed and built a system that consumes less than 50 W continuous wave (CW) and has been built into a briefcase. The system currently accommodates two incoming signals, yet the optical portion remains essentially unchanged as the number of independent signals, i.e., users, increases.

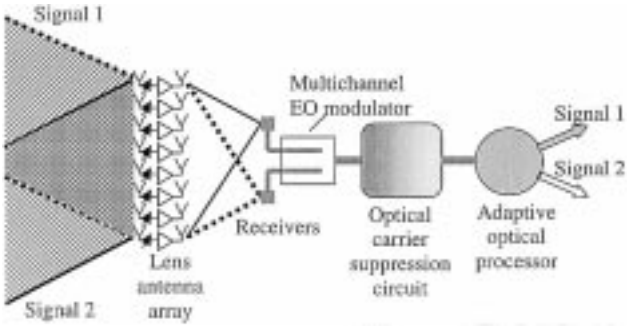

Fig. 1. Block diagram of the optically smart antenna array with two sources in the far field. The active receivers are positioned on the focal arc of the discrete lens antenna. The IF signals are then imposed onto the optical beam and processed by the adaptive optical circuit.

A block diagram of the adaptive receiver system is shown in Fig. 1, for the case of two incident signals modulated onto the microwave carrier. The front end consists of a 30-element 10-GHz constrained lens antenna array [3] with active antenna receivers positioned along the H-plane focal arc of the lens. Each receiver position corresponds to a specific direction of a plane wave incident and received by the lens array. Upon downconversion, the IF signals are imposed as phase modulation (PM) sidebands onto an optical carrier using electrooptic modulation. The optical carrier is then suppressed using an adaptive holographic element, leaving the signal-bearing optical sidebands. The modulated carrier-suppressed optical beams are coupled into the adaptive optical circuit, referred to as an "auto-tuning filter," that separates the two principal components of the signal input space. The outputs of the prototype adaptive antenna are baseband signals dynamically ordered by signal strength.

Principal component analysis (commonly referred to in the literature as PCA) is a second-order limiting case of the more general independent component analysis (ICA) [4]. Loosely speaking, the objective of independent component analysis is to extract one or more source signals of interest from a set of one or more received signals in the face of a relatively small number of statistical assumptions about the nature of the original sources (e.g., that the sources are statistically independent, hence the name ICA). Over the past two decades the field of ICA has produced a powerful collection of signal processing techniques that have been applied to signal separation, blind deconvolution, beamforming, jammer suppression, and a host

Manuscript received June 21, 2001; revised November 6, 2001. This work was supported in part by ONR and the Office of the Secretary of Defense through a MURI program in RF Photonics, Grant N00014-97-1-1006, and in part by the National Science Foundation under Grant PHY-9512150. The multidisciplinary integration of the components and related research is funded under an NSF Wireless Initiative under Grant ECS-9979355.

E. Fotheringham and D. Z. Anderson are with the Department of Physics and JILA, University of Colorado, Boulder, CO 80309 USA.

S. Römisch, P. C. Smith, D. Popovic, and Z. Popovic are with the Department of Electrical and Computer Engineering, University of Colorado, Boulder, CO 80309 USA (e-mail: zoya@colorado.edu).

Publisher Item Identifier S 0018-926X(02)05445-5.

of other spatio-temporal signal processing functions [5]. These techniques have been particularly successful in low-bandwidth applications such as speech processing. ICA techniques are less commonly found in RF communications and other high-bandwidth real-time signal processing applications because the computational overhead of ICA techniques is often higher than what is economically practical with current digital signal processing technology, as discussed in [6] for self-adaptive blind signal recognition.

The auto-tuning filter is an analog optical circuit that effectively performs principal component analysis, roughly by forming a correlation matrix and finding the largest eigenvalue and the corresponding eigenvector, which is referred to as the largest principal component of the input space. It also block-diagonalizes the matrix such that the temporal signal associated with the largest principal component is extracted from the input and everything else is passed through the filter. Principal component analysis in general and our optical circuit in particular, have their limitations; some are more fully discussed in Section V. For example, principal component analysis alone cannot reveal the original source signals when the eigenvalues of the correlation matrix are degenerate. The degeneracy must be resolved through higher order signal analysis.

Nevertheless, the optical circuit can perform its matrix computation with high-bandwidth signals (several gigahertz in the current circuit) and on vector spaces of very high dimension (a dimension of 2 here, but of order 10^4 in other works [7]. High-bandwidth, high-dimensionality signal processing is exceedingly challenging for digital signal processing approaches. A primary objective of our endeavor is to assess the design issues and tradeoffs associated with the incorporation of holographic optical signal processing in a microwave receiver. If the incorporation can be demonstrated as practical, then it seems appropriate to extend the optical processing capabilities, for example, by developing higher order signal processing optical circuitry. The prototype receiver presented here is our first such end-to-end, "packaged" demonstration.

The design, operation and measured performance of each of the three subsystems indicated in the system block diagram in Fig. 1 are given in the following sections, with a subsequent section on end-to-end assessment of the adaptive antenna prototype. The operations performed on the incident signals are traced through: 1) the microwave front end, 2) the electrooptic modulation and carrier suppression stage, and 3) the optical processing (auto-tuning filter) stage. In the last section of the paper we discuss the implementation of an extension of the two-receiver system to an N-receiver adaptive array and the implications of using an optically smart quasi-optical antenna array in wireless communications.

II. The Microwave Front End

The lens antenna array shown schematically in Fig. 1 is a quasi-optical array analogous to a Rotman lens. Such active (transmit and receive) T/R lenses have recently been demonstrated to improve dynamic range, increase effective radiated power (ERP) by spatial combining and improve reliability, e.g., [8], [9]. In this work, a passive discrete 10-GHz lens with 30 patch antenna elements is used, in which the focusing is accomplished with varying delay lines across the array between input and output antenna elements. The photograph of one side of the lens, Fig. 2, shows the patch antenna elements fed at the nonradiating edges and the microstrip delay lines, which are connected with via holes to the orthogonally polarized patches on the other side of the two-layer lens array. Orthogonal polarization improves the isolation between the two sides of the lens. The measured and calculated half-power beamwidths in the copolarized E- and H-planes are 15°, the cross-polarization ratio at boresite is higher than 20 dB, resulting in a directivity of about 22 dB.

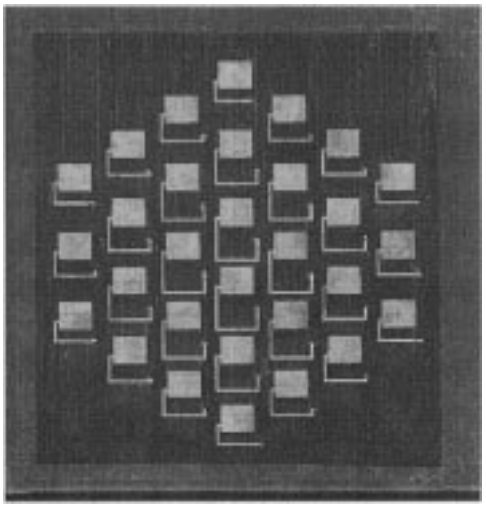

Fig. 2. Photograph of one side of a 30-element *X* band two-layer quasi-optical lens antenna array with patch antenna elements. The array lattice is triangular with an element size of 0.63 by 0.83 free-space wavelengths at 10 GHz. The feed lines vary in length across the array, producing a focal surface. The feed lines are connected with via holes to orthogonally polarized patch antennas on the other side of the two-layer array.

The F-number of the lens is 0.6, corresponding to a focal length of 7.5 cm. The array lattice is triangular, with a period of $0.65\lambda_0$, chosen to minimize grating lobes when the beam is scanned. The lens has a number of imperfect focal points and in this demonstration we use two of these points along the H-plane focal arc to place receivers, each preferentially receiving one spatial beam. The isolation, or "crosstalk," between the imperfect focal points for two signal sources was measured using the setup shown in Fig. 3(a). The two sources have equal-power levels at frequencies f_1 and f_2, which are within the bandwidth of the lens array and the receiving antennas on the focal arc. The two transmitters are in the far field equally away from the lens array and copolarized with the receiving side of the lens array. The angle between the optical axes and the line-of-sight corresponding to each transmitter is β. The receiver is translated along the focal arc and signal powers are measured for different angles α in Fig. 3. For positions where $\alpha = \beta$, the receiver preferentially receives from one of the sources, but some amount of signal power from the other source is also present and referred to as the "crosstalk" signal. The relative amount of the crosstalk depends on the spatial separation between the sources and is shown in Fig. 3(b)–(d). In most cases, the level of cross-talk is below 20 dB, e.g., when the transmitters are at $\pm 15°$ off the lens

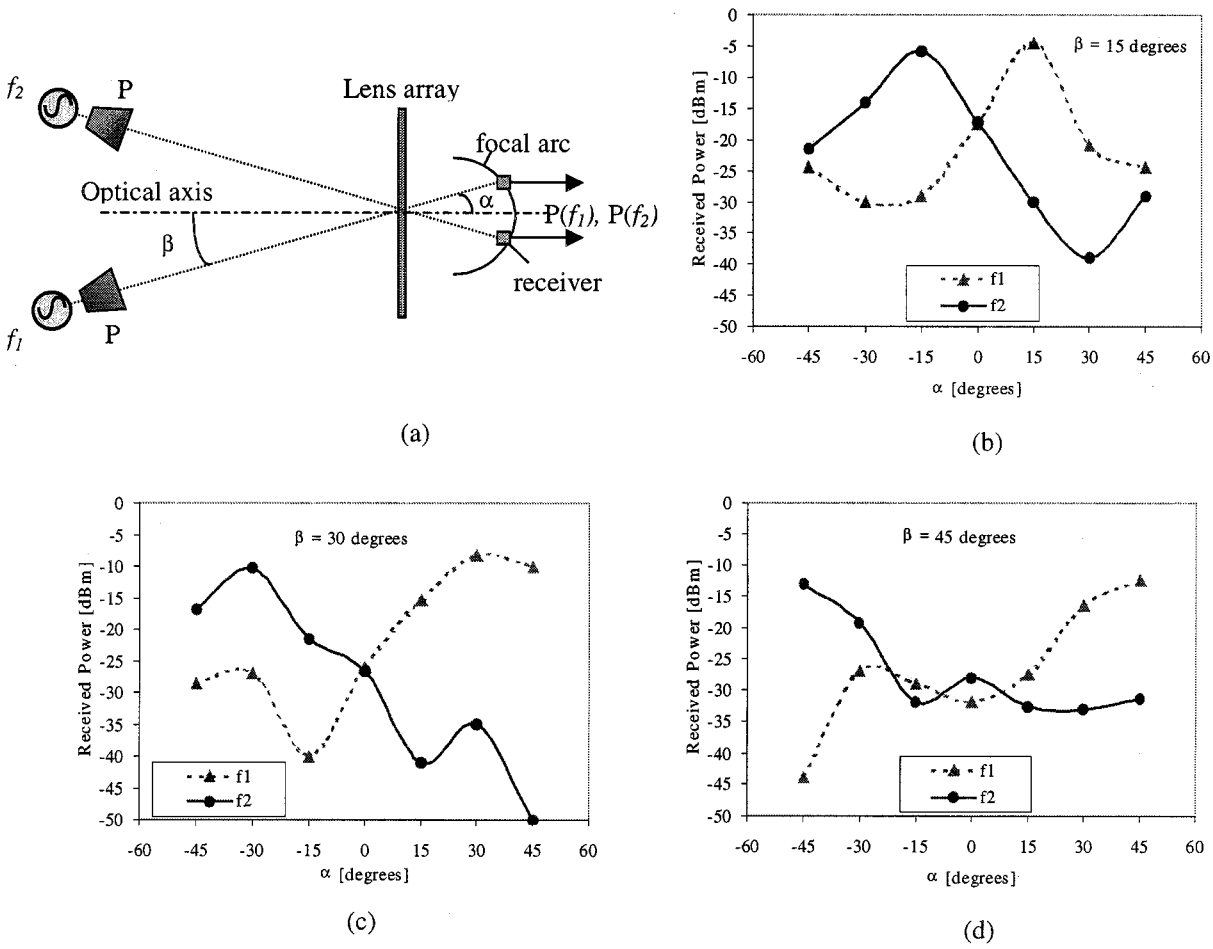

Fig. 3. (a) Schematic of measurement setup used to characterize the multiple-receiver lens antenna array. Each transmitting antenna is located 0.8 m from the lens and transmits 25 dBm at frequencies 10 MHz apart around 9.9 GHz. Measured "crosstalk" between the two signals as a function of the receiver position along the focal arc (α) for different transmitter position. (b) $\beta = 15°$. (c) $\beta = 30°$. (d) $\beta = 45°$.

optical [Fig. 3(b)], the receivers placed at the corresponding positions will receive the two signals with a contrast ratio of about 25 dB. The contrast ratio depends on the radiation pattern of the lens. For example, Fig. 3(c) shows an asymmetry of about 10 dB around boresight, consistent with the measured asymmetric radiation patterns of this particular lens (which has a null at $+30°$, but not at $-30°$).

Each receiver is an active integrated antenna followed by a down-conversion stage, the block diagram of which is shown in Fig. 4. An RT/Duroid substrate with a high relative permittivity of $\varepsilon_r = 10.5$ (0.508 mm thick) is used in order to reduce the size of the integrated active antennas. The antennas are designed for 10 GHz (6.3 mm by 4.3 mm), with a 2:1 voltage standing wave ratio (VSWR) bandwidth of about 150 MHz. The antenna feed is connected directly to a low-noise amplifier (LNA) for optimal noise figure (CHA2063 united monolithic semiconductors, with a 7–13-GHz bandwidth, 16-dB gain, and 2-dB noise figure). Fig. 5 shows the measured gain of the active antenna at the output of the LNA and the measured return loss of the patch, indicating that the receiver bandwidth is determined by the antenna and that the gain contributed by the LNA is not sacrificed. The output power for the LNAs at 1-dB-compression point is

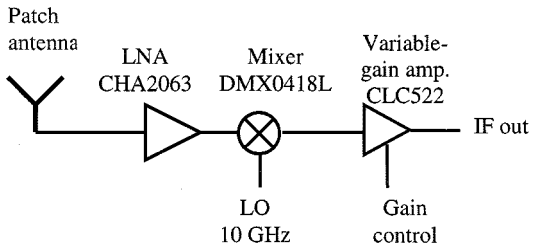

Fig. 4. Block diagram of receiver positioned on the focal surface of the lens array.

10 dBm, with low dc power consumption (40 mA at 5 V). A mixer downconverter follows the LNA. The IF amplifiers are CLC522 national semiconductors wideband variable gain amplifiers and they provide more than 40 dB gain control through a single high-impedance voltage input.

The ability to control the levels of the signals at the input of the optical processor is important for proper optical processing, as discussed in Section III. The output of the IF amplifiers drives power amplifiers, the outputs of which drive the electrooptic modulator (EOM). The test signals used for characterizing the components of the adaptive array are

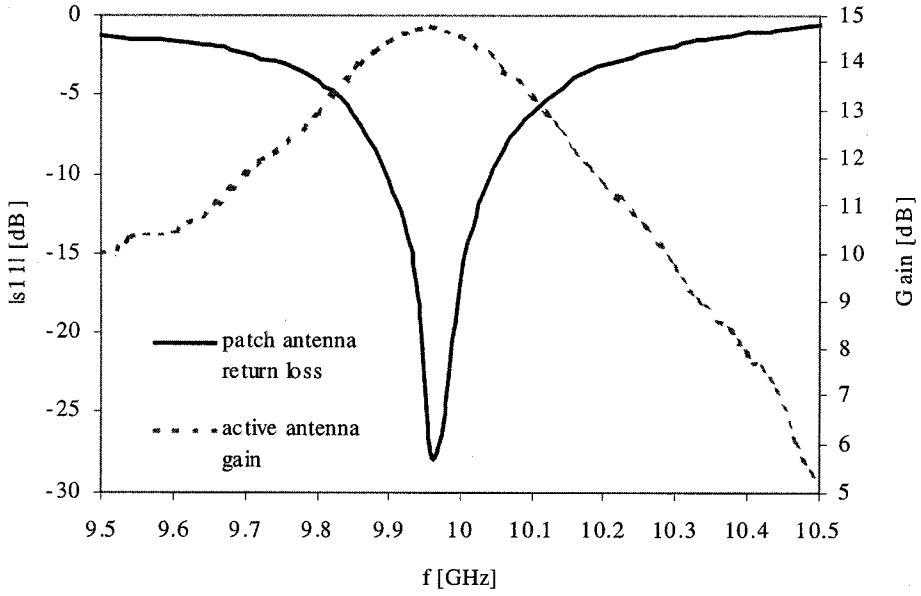

Fig. 5. Measured return loss of receiver patch antenna (solid line) and gain of active antenna at the output of the LNA (dashed line).

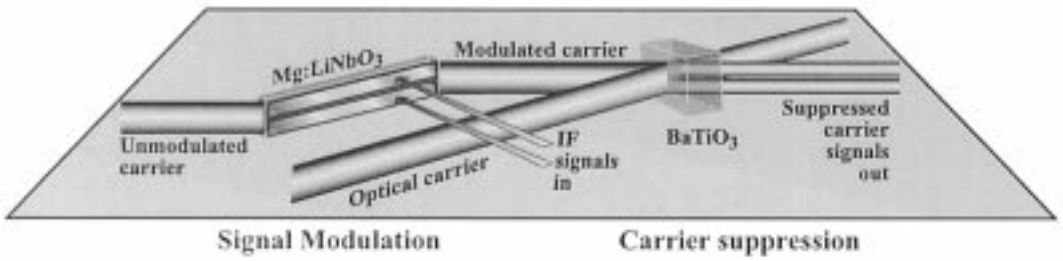

Fig. 6. Schematic of the EOM and carrier suppression circuits.

two signals at 128–130 MHz up-converted to the 10-GHz microwave carrier. In fact, the IF signals can share the same spectrum; we use two signals at the different IF frequencies only to simplify the measurement.

III. Electrooptic Modulation and Carrier Suppression

The IF signals are encoded as phase-modulation sidebands on an optical carrier having a wavelength of 532 nm using a multichannel electrooptic crystal modulator, shown in Fig. 6. The input beam is formed into a vertical line segment. It passes through a magnesium-doped lithium niobate crystal with two vertically separated signal electrodes on one side and a ground plane on the other. Hence, the upper and lower portions of the beam are modulated by different IF signals giving a spatially as well as temporally modulated output beam.

The electrooptic crystal is a thin slab (0.7 mm by 5.2 mm by 45.5 mm) with the optical faces cut at Brewster's angle (about 65°) in order to minimize reflections. The two signal electrodes are copper strips, approximately 2 mm wide and separated by about 1.5 mm from each other. At the operating IF frequency of 130 MHz, the modulator is a lumped-element circuit. The modulation efficiency is measured to be about 0.2 rad/V for both electrodes, fed separately with narrow-band matching circuits. The crosstalk (S_{21}) between the two electrodes, measured with a HP8510 network analyzer, is -24 dB.

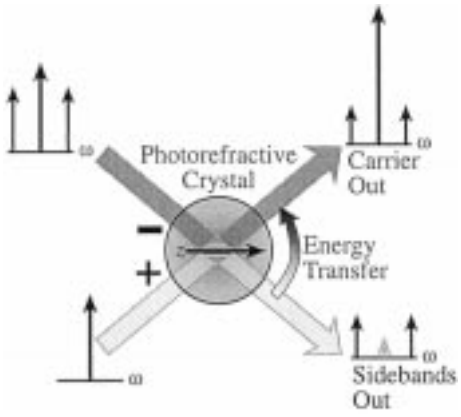

Fig. 7. Schematic diagram of two-beam coupling carrier suppression. The input to the minus ("−") port is a modulated laser beam while the input to the plus ("+") port is an unmodulated beam from the same laser. Nonlinear coupling between the beams causes the energy in the carrier at the minus port to be transferred to the plus port at the output.

The auto-tuning filter is the adaptive heart of the system. We have earlier mentioned that it extracts the principal component of the ensemble of signals. It does so partly by assessing the degree of correlation among the various signals. The optical carrier is common to all the signal channels and therefore introduces an unwanted correlation. To eliminate this correlation, we suppress the optical carrier using two-beam coupling

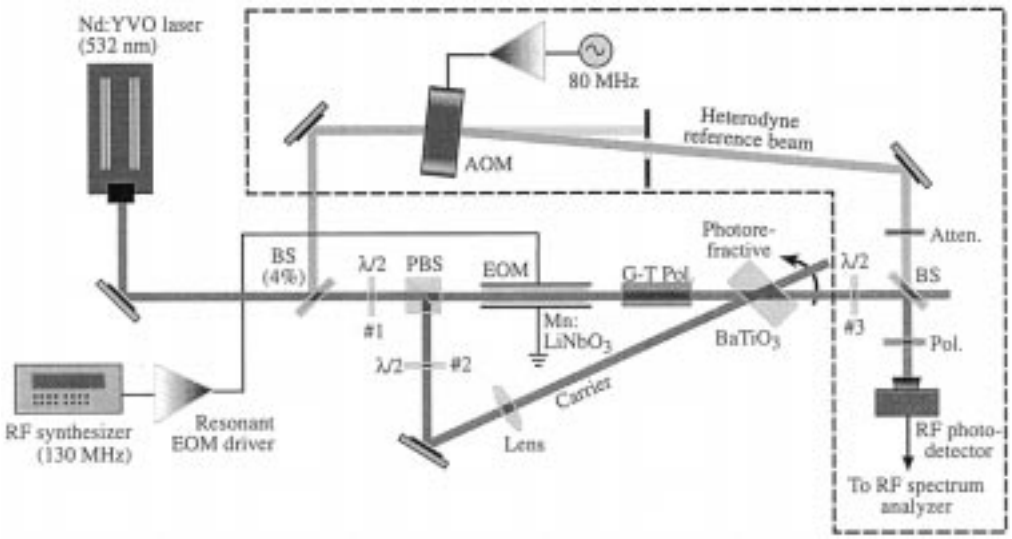

(a)

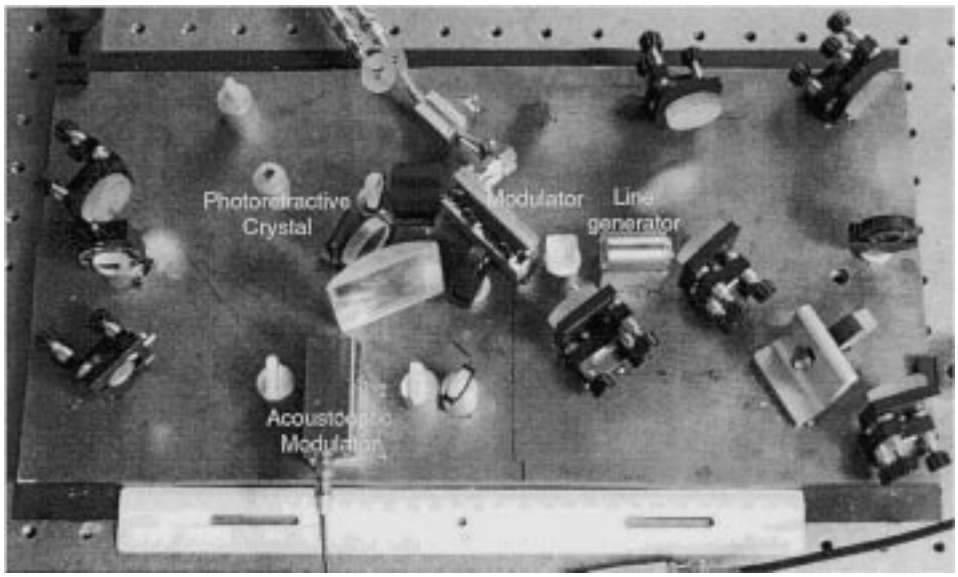

(b)

Fig. 8. (a) Block diagram and (b) photograph of optical carrier suppression system including the heterodyne measurement branch highlighted by a box. A line generator (LG) is used to produce the line-shaped beam required by the electrooptic modulator. L1 is a spherical lens ($F = 250$ mm.), while all other lenses are cylindrical. All optics in the dotted box are part of the heterodyne apparatus used to quantify the carrier suppression.

within a barium titanate photorefractive crystal [10], [11]. A more common optical interferometric approach using a Mach–Zehnder interferometer, e.g., [12] typically achieves 30–35 dB of suppression and requires electronic adaptive feedback for good performance. The system presented here achieves over 60 dB of suppression and is inherently optically adaptive. A complete treatment of photorefractive carrier suppression principles is beyond the scope of this work and is given in [13]. Here we present only the fundamentals of operation and the results relevant to our system.

The beam-coupling interaction takes place between two beams coming from the same laser, one of which has been modulated with the IF signals by the EOM as illustrated in Fig. 7 and schematically in Fig. 8. As a result of the interaction the modulated beam is transmitted from the crystal with the optical carrier largely suppressed, while the other beam has increased carrier power and also a portion of the IF signal power.

As suggested by Fig. 7, carrier suppression comes at the cost of some signal power lost to the plus port of the photorefractive crystal. For modulation strengths less than unity, about 3 dB of signal power is lost from the signal-bearing beam. There is additional loss in the photorefractive crystal itself, which varies among crystals and is in our case about 1.5 dB.

The experimental prototype modulation and carrier suppression subsystem is shown in Fig. 8(a); the dotted portion indicates the measurement apparatus used to assess suppression performance. The photograph of the system is given as Fig. 8(b). The input laser is a Coherent Inc. Verdi laser operating at 532 nm. The laser beam is formed into a line segment using a line generator followed by a cylindrical lens. The beam is then split by a polarizing beamsplitter/half-waveplate combination

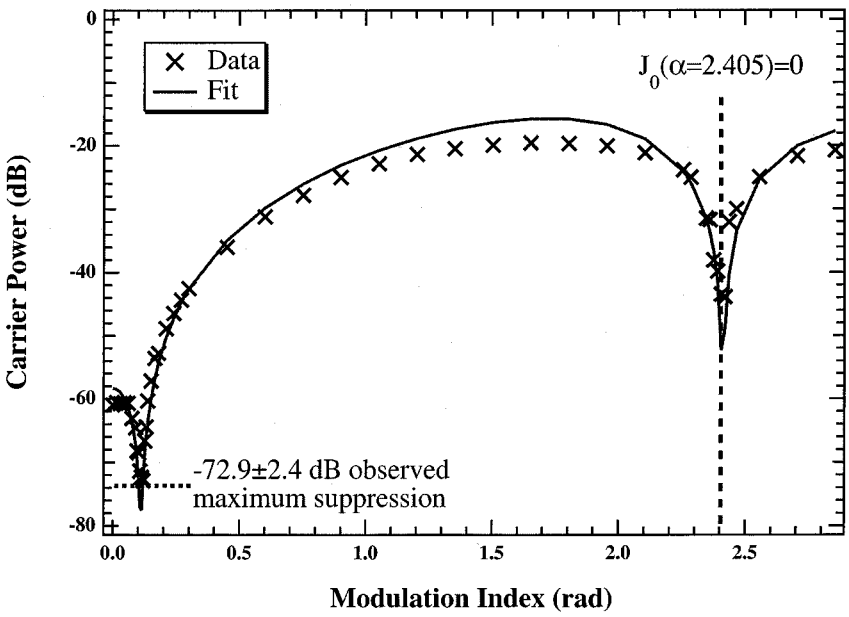

Fig. 9. Measured performance of carrier suppression by two-beam coupling (crosses) and comparison with theory (solid curve).

to provide an adjustable power ratio. One of the beams enters the EOM, then continues to the photorefractive barium-titanate crystal ($BaTiO_3$). A small fraction of the other beam is used for measurements, as described below. The larger fraction interacts with the modulated beam for carrier suppression in the photorefractive medium. The optical powers at the input face of the crystal are adjusted to be approximately equal. A second half-waveplate is used to rotate the polarization of the unmodulated beam to that required for two-beam coupling.

The performance of the carrier suppression system is determined using a heterodyne technique. The measurement beam is frequency shifted by 80 MHz from the carrier by an acoustooptic modulator. The measurement beam and the carrier-suppressed beam are then combined with a 50/50 beamsplitter, detected by a broadband detector and the spectrum is measured using an RF spectrum analyzer. The heterodyne signal allows us to determine the power of the optical carrier in the modulated beam, as well as the strength of the various sidebands.

The EOM is calibrated by finding the drive voltage for which the output carrier power vanishes, i.e., by finding the first zero of the zero-order Bessel function, corresponding to a modulation index $\alpha \cong 2.405$. Once calibrated, the modulator drive voltage is used to set the value of m, the ratio of power in the sidebands to the total power of the modulated laser beam. The data in Fig. 9 shows the experimentally measured carrier suppression as a function of modulation strength m along with a curve calculated from photorefractive theory [13]. Note that the right-hand minimum in the curve corresponds to the first zero of the zero-order Bessel function. The one of interest is the left-hand minimum, which corresponds to the theoretical perfect suppression. The shape of the theoretical curve agrees qualitatively well with the theoretical curve. The maximum observed value of about -73 dB is measurement limited and is more than sufficient to meet the current needs of the system. The measured limit arises from a combination of detector noise and carrier feedthrough in the acoustooptic modulator.

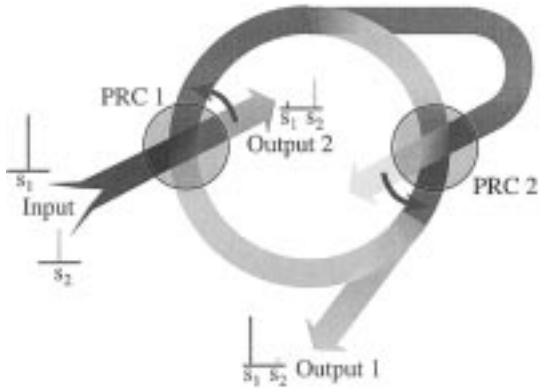

Fig. 10. Schematic diagram of the auto-tuning filter. Two photorefractive crystals (PRCs) are interconnected in a reflexive oscillator configuration. The strongest independent component of the ensemble of input signals is extracted at Output 1 while the remainder appear at Output 2.

IV. Auto-Tuning Filter

The auto-tuning filter is a self-organized system that extracts the principal component of the input signal space [7]. The filter has one input and two outputs. The input consists of multiple IF signals imposed on an optical beam as described above. One output (#1 in the schematic Fig. 10) provides the strongest IF principal signal component and the other (#2 in the same figure) provides all the other components. The output of interest depends on the application: for example in case of a weak signal and a strong interferer, *output 2* extracts the wanted signal. In case of a signal barely above noise level, *output 1* delivers the signal with suppressed noise. It is fundamentally an optical oscillator where gain is supplied by photorefractive two-beam coupling. There are two photorefractive interactions in the oscillator: the gain interaction and another that is referred to as a reflexive interaction.

In the interaction that is taking place in the crystal of the gain unit (PRC 1 in the figure) the strong input beam primarily pro-

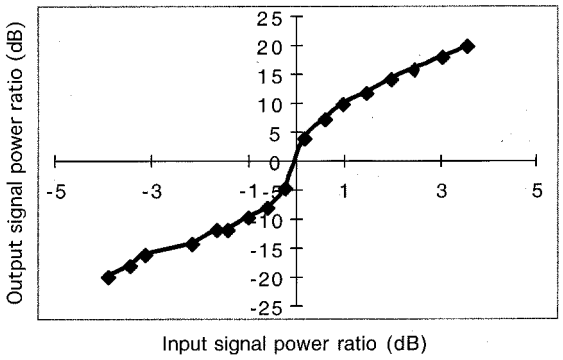

Fig. 11. Measured signal enhancement provided by the auto-tuning filter. We define signal enhancement as the power ratio of the two signals at the output divided by their power ratio at the input.

Fig. 12. Photograph of the auto-tuning filter used in the adaptive antenna system.

vides energy to the oscillating beam. The reflexive coupling interaction that takes place in the second crystal, PRC 2, enhances the contrast between the two principal components: one initial beam is split in two unequal parts that then interact by two-beam coupling. If the optical beam is carrying statistically independent IF signals, the dynamics of reflexive coupling is such that the gain experienced by each optically carried IF signal is proportional to its power (*output 1*). Thus, the stronger the signal, the more gain it undergoes. The gain loop provides feedback to the reflexive-coupling unit, enhancing the competition for gain until the signal that was initially the strongest dominates the oscillation in the loops. In Fig. 10, *output 1* provides the oscillation signal, while *output 2* has the stronger signal suppressed.

The auto-tuning filter was designed, built and then characterized with narrow-band test signals at about 80 MHz, with the two signal frequencies differing by less than 1 kHz. Two acoustooptic modulators (AOs) provide the frequency modulation of a diode-pumped frequency-doubled Nd:YAG laser beam (532 nm). Although AOs have the drawback of being narrow-band devices, they offer the advantage of providing modulated signals without the carrier. It was therefore possible to test the optical processor separately from the carrier suppression circuit. The signal-bearing beams from each of the two modulators are launched together into the auto-tuning filter.

The curve displayed in Fig. 11 shows the signal enhancement provided by the auto-tuning filter. We define signal enhancement as the power ratio of the two signals at the output divided by their power ratio at the input. The interesting region of this plot is the slope around the origin: when the input signals are exactly equal in power, the filter cannot choose one or the other; but as soon as the input ratio differs from 0 dB, the filter becomes capable of extracting the stronger one. For instance, an input ratio of 1 dB produces a 7-dB ratio at the output, providing an enhancement of 6 dB. The signal enhancement reaches a maximum of about 30 dB.

A photograph of the auto-tuning filter used for the adaptive antenna processing is shown in Fig. 12; a U.S. quarter dollar is shown in the background for scale. The signal processing bandwidth of the photorefractive auto-tuning filter is determined by the oscillator's round-trip path length. Here the round-trip path length is approximately 5 cm, corresponding to an allowed signal bandwidth of about 6 GHz. The actual signal bandwidth of the entire system is limited by the optical modulator electronics to about 10 MHz.

V. End-to-End Characterization of the Prototype

The adaptive processor separates the two principal components of the incoming signal space. A complete discussion of principal component analysis and of the corresponding properties of the processing system is beyond the scope of this work. Here we provide a qualitative description as a context in which to present the quantitative measurements given below.

In general, one usually wishes to extract one or more of the originally transmitted source signals in the face of multipath and other interference effects. The outputs of our two-channel system do not, in general, recover the original source signals. Rather, the output of the adaptive processor always provides the principal components of the signal space. The principal components are proportional to the two transmitted signals if and only if three conditions are satisfied: 1) the sources are independent, 2) they produce different received powers, and 3) the signals incident on the optical processor correspond to *spatially orthogonal* signals. Condition 1 is always satisfied in practice unless some spurious effect causes an apparent correlation (such as the presence of the optical carrier, in our case). The limits imposed on our system by condition 2 are already revealed by the signal extraction curve of Fig. 11, which shows a finite slope through the origin. As indicated in the Section I, this requirement reflects a fundamental limitation of principal component analysis. In principle, condition 2 could be relaxed with a more sophisticated optical circuit capable of higher order (than correlation) signal processing. The fact, though, is that this requirement is usually satisfied in practice. Condition 3 is another matter. It reflects a particular limitation of our holographic circuit that could be relaxed with a different but more complicated optical circuit geometry. As it stands, condition 2 is the most confining one and is the focus of the end-to-end characterization of the system.

Qualitatively, one expects that the principal components will become more and more a superposition of the two source signals as the transmitters are moved close together in angular space. When they are at the same angular position, there is nothing

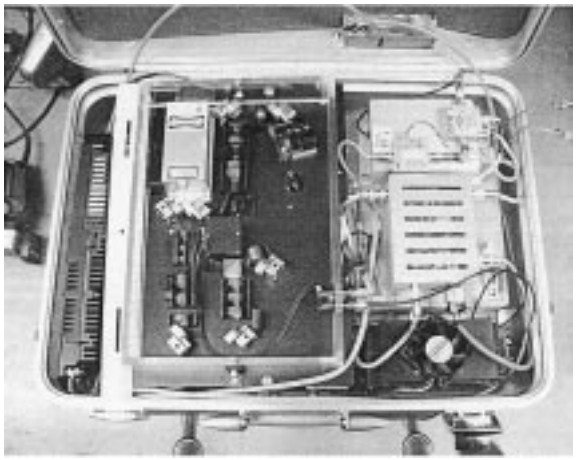

(a)

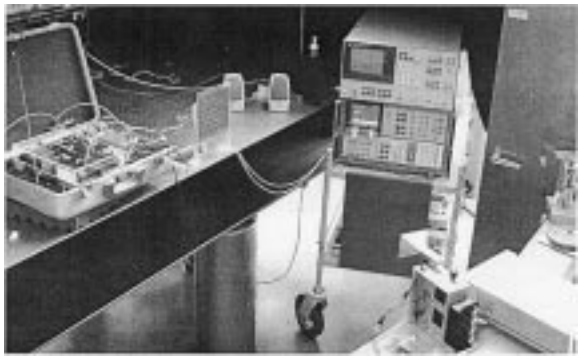

(b)

Fig. 13. (a) The adaptive receiver system packaged in an aluminum briefcase. (b) Antenna system measurement arrangement with one transmitter shown in the front-right and another partially shown in the center-right. The antenna array and packaged processing system may be seen on the table on the left.

available to the optical processor to distinguish one source from two sources.

Fig. 13(a) is a photograph of the adaptive antenna processing system. The system is packaged in an aluminum briefcase with a single power plug. The electronic portions of the system sit on the right side of the case, while the optical portion sits to the left of center. The laser power supply is visible at the far left, while the other power supplies, as well as two cooling fans, lie under the electronics. Fig. 13(b) shows the system as it has been tested end-to-end. The processor sits toward the left of the photograph, with the antenna lens array sitting just to its right. On the lower right is a transmitter with a horn antenna and a second transmitter is partially visible on the far right and vertical middle of the photograph. The two transmitters are placed symmetrically about the antenna array boresite.

We assessed the performance of the system by taking signal extraction curves reminiscent of the enhancement curve shown in Fig. 11 for three different angles between the two transmitters. Fig. 14 provides a context in which to describe the measurements. In general, each of the two detector outputs will be composed of a linear superposition of the transmitter signals. Since the transmitted signals are uncorrelated, one can write

$$R_1 = R_{11} + R_{12}$$
$$R_2 = R_{21} + R_{22}$$

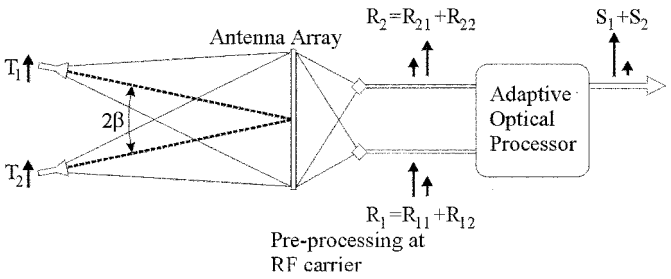

Fig. 14. Schematic defining the context of the end-to-end system measurements.

TABLE I
CROSSTALK AND ENHANCEMENT SLOPE OF THE ANTENNA SYSTEM FOR THREE DIFFERENT ANGLES BETWEEN THE TRANSMITTERS IN THE FAR FIELD

Angle between transmitters (α) [degrees]	Receiver cross talk [dB]	Maximum slope enhancement (dB)
48	-15	76
35	-10	6.1
20	0	1.3

where R_{jk} is the received signal power from transmitter T_k after downconversion to the IF. With a large angle between the transmitters, the received power R_1 at the IF on one channel of the receiver is primarily from transmitter T_1 while the received power R_2 at the other channel is primarily from transmitter T_2. In other words, for equal transmitted powers R_{12} and R_{21} are small compared to R_{11} and R_{22}. We measure a "crosstalk" between receiving channels by setting the transmitter so that the received powers R_{11} and R_{22} are equal and then determine $C_j = R_{jk}/R_{jj}$ $(i \neq k)$. From the symmetry of our experimental arrangement, we expect the two values of crosstalk to be the same, $C_1 \approx C_2 \equiv C$. Table I shows this crosstalk C for each of three angles. At the largest angle of 48° between the transmitters the crosstalk is -15 dB. At the smallest angle of 20° it is 0 dB.

In order to keep the presentation of the quantitative data relatively simple, we define a single-input signal power ratio, R_{11}/R_{22}. At the output, the auto-tuning filter provides the principal components of its input signals. In this experiment, we optically detect only the power from output 1 which provides the higher power of the two principal components. We define a single output power ratio S_1/S_2, the ratio of detected power corresponding to transmitter T_1 to the power corresponding to transmitter T_2. Ideally, this output ratio would be zero or infinity, depending on which signal was larger, that received from T_1 or that received from T_2, but otherwise independent of the input ratio. Fig. 15 plots the output signal ratio versus the input ratio for three different angles between the transmitters. The two curves for the larger angles have a characteristic "S" shape. When the received signals have identical powers they are indistinguishable by the auto-tuning filter (this is

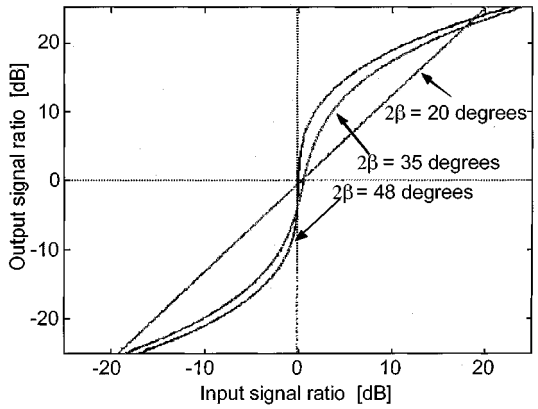

Fig. 15. Signal extraction properties of the adaptive system parameterized by the mutual angle between the transmitters.

because the two eigenvalues of the signal correlation matrix are degenerate). However, even a small power difference can provide the needed distinction. Of particular interest therefore is the slope near the origin of the curve. For the largest angle of incidence it is 76 dB/dB. This means that if the signals differ by 0.04 dB at the input to the auto-tuning filter, their ratio is enhanced to about 3 dB at the output. Once the output ratio is above 10 dB or so, the enhancement begins to level off. With the smaller angle between the transmitters of 35° the "S" curve becomes much shallower. The slope at the origin is 6.1 dB/dB. At an angle of 20° the "enhancement" is small. At the origin it is about 1.3 dB/dB.

At this latter angle we note that the crosstalk is 0 dB, meaning that all four IF powers R_{jk} are about the same size for equal transmitted powers. It would seem for this smallest angle that the two transmitters are unresolved by the antenna and therefore their two signals should be indistinguishable from one. However, the analysis in terms of power omits the important role of the signal phase and this is the reason there is still some observed signal contrast enhancement, however small.

VI. Discussion

A number of remarks are in order concerning this prototype demonstration and the potential role of adaptive optical processing in wireless communications. The adaptive processing in the prototype developed in this work is performed by a relatively simple optical circuit. The inherent function of this circuit is principal component extraction and it has been effectively demonstrated. It is useful to note that the role of the antenna lens array in our system design is more subtle than might first be apparent. It is true that the array performs something akin to a spatial Fourier transform on the signal space; roughly speaking it converts an angle of arrival to a spatial region in the focal surface. In this sense it does some preprocessing of the incoming signals. If the incoming signals are known to have well-defined and distinguishable directions, the adaptive processor is unnecessary. The focal-surface detectors already contain well-separated signals. That does not help in cases of multipath and other forms of interference, however. In principle it makes no difference to the auto-tuning filter whether or not this "Fourier" transformation of the signals takes place. The actual practical benefit of the antenna lens array enters through dynamic range considerations. In a typical communications scenario one can expect the power incident on the antenna lens array to be more or less uniform over the array, while the power at the focal surface varies by a larger amount. Consider two angularly well-separated sources for example, one giving rise to a received power of 1 W and the second giving rise to a received power of 0.1 W. At the array, each antenna element receives the same power of $1.1/N$ watts, where N is the number of array elements. At the focal surface, one detector receives 1.0 W while the second receives 0.1 W. One can clearly amplify the signal from the second detector so that the output power from the front end is the same for both signals. This could not be done were the signals taken directly at the antenna array. Such dynamic range considerations tend to remain valid when the signals are subject to a multipath environment.

Our prototype demonstration is designed for processing two signals. Among the major benefits of the optical processing is its scaling characteristics. A larger input signal space, say of size N, can be accommodated merely by increasing the number of electrodes on the electrooptic modulator to N the auto-tuning filter remains largely unchanged. Increasing the number of output channels from 2 to M, requires a total of $(M-1)$ auto-tuning filters. Thus, in general the adaptive processor scales linearly with the size of the desired signal space, rather than quadratically, as is often the case with adaptive electronic processors.

The system will optimally process multipath communication signals provided arrival time differences are negligible compared to the inverse bandwidth of the signal. Different paths are received by different focal surface receivers. Automatic gain control normalizes the received signal strengths to the same level and the auto-tuning filter combines the received signals coherently while the noise from different receivers adds incoherently. When the multipath delay times are much greater than the inverse signal bandwidth, the auto-tuning filter treats each as a separate source and extracts the strongest one.

The prototype demonstrated here processes signals with bandwidths in the 100 MHz range. None of the components are however limited to this bandwidth. Broad-band antennas, such as second resonant slots with up to 20% bandwidth can be used instead of the patches at a higher carrier frequency [4], allowing for several gigahertz IF frequencies. A possible issue in this case may be the angle-of-arrival detection quality due to higher grating lobes at the lower band edge, which is a design parameter. The electrooptic modulator presented here is effectively a lumped-element circuit, but its architecture accommodates a set of N coupled travelling wave transmission lines and such an EO modulator can cover several gigahertz of bandwidth with good modulation efficiency.

In summary, this paper describes a smart antenna array with optical adaptive processing. The array operates at a 10 GHz RF carrier and a 125-MHz IF signal. The input wave is an unknown superposition of a number of uncorrelated signals incident from different directions and with possibly changing

spatial and temporal characteristics. The output electrical signals are adaptively separated and ordered according to their respective signal strengths. This functionality is accomplished with a compact holographic optical processor, which is completely internal to the system. The processor and associated electronics is packaged in a standard-size aluminum briefcase with a single external power plug and consumes less than 50 W of CW power.

ACKNOWLEDGMENT

We thank L. Czaia from the University of Colorado for help in crystal fabrication.

REFERENCES

[1] D. Z. Anderson, V. Damiao, E. Fotheringham, D. Popovic, S. Romisch, and Z. Popovic, "Optically smart active antenna arrays," in *Proc. IEEE IMS Dig.*, Boston, June 2000, pp. 843–846.

[2] G. T. Okamoto, *Smart Antenna Systems and Wireless LANS*. Norwell, MA: Kluwer , 1999.

[3] D. T. McGrath, "Planar three-dimensional constrained lenses," *IEEE Trans. Antennas Propagat.*, vol. AP-34, pp. 46–50, Jan. 1986.

[4] P. Comon, "Independent component analysis, A new concept?," *Signal Processing*, vol. 36, pp. 287–314, Apr. 1994.

[5] S. Haykin, *Unsupervised Adaptive Filtering, Volume 1: Blind Source Separation*. New York: Wiley, 2000.

[6] C. Roland and J. Palicot, "A blind recognition of the transmitted signal for a self-adaptive re-configurable terminal," in *Proc. IST Mobile Communication Summit*, Barcelona, Spain, Sept. 9–12, 2001.

[7] M. Saffman, C. Benkert, and D. Z. Anderson, "Self-organizing photorefractive frequency demultiplexer," *Opt. Lett.*, vol. 16, no. 24, pp. 1993–1995, Dec. 1991.

[8] S. Hollung, A. Cox, and Z. Popovic, "A quasioptical bi-directional lens amplifier," *IEEE Trans. Microwave Theory Tech*, vol. 47, pp. 2352–2357, Dec. 1997.

[9] Z. Popovic and A. Mortazawi, "Quasioptical transmit/receive front ends," *IEEE Trans. Microwave Theory Tech.*, vol. 48, pp. 1964–1975, Nov. 1998.

[10] P. Yeh, *Introduction to Photorefractive Nonlinear Optics*. New York: Wiley, 1993, ch. 3.

[11] D. Z. Anderson and J. Feinberg, "Optical novelty filters," *IEEE J. Quantum Electron.*, vol. 25, pp. 635–647, Mar. 1989.

[12] R. Montgomery and R. Desalvo, "A novel technique for double side-band suppressed carrier modulation of optical-fields," *IEEE Photonics Technol. Lett.*, vol. 7, pp. 434–436, Apr. 1995.

[13] D. Z. Anderson, V. Damiao, D. Popovic, Z. Popovic, S. Romisch, and A. Sullivan, "−70 dB optical carrier suppression by two-beam coupling in photorefractive media," *J. Appl. Phys. Invited*, pp. 743–748.

Edeline Fotheringham was born in Lima, Peru, in 1975. She received the electrical engineering diploma from I'Ecole Nationale Superieure de Physique de Strasbourg, France, in 1998 and the Diplome d'Etudes Approfondies in photonics from the Universite Louis Pasteur (also in Strasbourg). She is currently working toward the Ph.D. degree at JILA and the Department of Electrical and Computer Engineering at the University of Colorado, Boulder.

Her research interests include photorefractive nonlinear optical circuitry for microwave signal processing.

Stefania Römisch was born in Torino, Italy, in 1967. She received the electrical engineering degree and the Ph.D. degree in electronic instrumentation both from Politecnico di Torino, Italy, in 1993 and 1998, respectively.

In 1994, she was a Consultant with the Electronic Department of Politecnico di Torino, and a Guest Researcher in the Time and Frequency Division of National Institute of Standard and Technology (NIST), in Boulder, CO. In 1998 and 1999, she was a Guest Researcher in the Time and Frequency Division at NIST, where she worked on optoelectronic oscillators. She is currently a Research Associate with the Department of Electrical and Computer Engineering, University of Colorado, Boulder, where she is involved with optical processors for smart antenna arrays and is presently designing *Ka*-band lens arrays for satellite communications. Her research interests include low-noise microwave oscillators, analysis of noise processes and noise measurement systems, optoelectronic systems, antenna design, and frequency metrology.

Paul C. Smith was born in Colorado. He received the B.S. and M.S. degrees in electrical engineering from the University of Colorado at Boulder, in 2000. He is currently working toward the Ph.D. degree at the same university.

In 2001, he worked as a Researcher on high-speed electrooptical analog to digital conversion with the Daimler Chrysler R&D center in Ulm, Germany. He has also worked on Web-based learning programs for fiber optics and circuits courses. His research interests include VCSEL arrays for optical backplanes and nonlinear optical processors for *X*-band signals.

Mr. Smith has been a member of the Eta Kappa Nu, Tau Beta Pi, and the Golden Key Honor Societies

Darko Popović received the Dipl. Ing. degree from the University of Belgrade, Yugoslavia in 1995. He is currently working toward the Ph.D. degree in electrical engineering at the University of Colorado, Boulder.

From 1995 to 1998, he was a Research Assistant at the Institute of Physics, Belgrade, Yugoslavia. He worked at the National Institute of Standards and Technology, Boulder, on the design of a new generation of atomic clock synthesizers on an exchange visitor program in 1998. His research interests include microwave active antennas, microwave communications, and RF photonics.

Dana Z. Anderson received the B.S.E.E. degree from Cornell University, Ithaca, NY, and the Ph.D. degree in physics from the University of Arizona at Tucson, in 1975 and 1981, respectively.

He was with the California Institute of Technology, Pasadena, for three years as a Research Associate working on a prototype gravitational wave optical interferometer. During this time, he developed a precision measurement reflectometry technique for ultra low-loss mirrors. This technique is now widely used in industry and research laboratories. He is currently a Professor of Physics at the University of Colorado, Boulder, where he is extensively involved in laser gyroscopes and has served as a Consultant to Litton Guidance and Control Systems and Rockwell, International. He has also developed a new class of optical techniques for information processing based on dynamic holography and is also developing the technology in a new field called fiber atom optics which uses laser light to guide atoms through hollow-core optical fibers.

Prof. Anderson was awarded the Optical Society of America's R. W. Wood Prize in 1994 . He was a National Science Foundation Presidential Young Investigator. He is a Fellow of JILA, a Fellow of the Optical Society of America, and of the American Physical Society. He is also an A. P. Sloan Research Fellow and has served as Topical Editor for *Optics Letters*, *Optics Communications*, and the *International Journal of Neural Networks*. In 2001, he received an Alexander von Humboldt Research Award.

Zoya Popović (SM'99–F'02) received the Dipl. Ing degree from the University of Belgrade, Yugoslavia, and the Ph.D. degree from California Institute of Technology, Pasadena, in 1985 and 1990, respectively.

Since 1990, she has been a Professor at University of Colorado, Boulder. She is a coauthor of a textbook and workbook entitled *Introductory Electromagnetics* (Englewood Cliffs, NJ: Prentice-Hall, 2000) for which she received the ASEE Hewlett Packard Terman Award in 2001. She is also coeditor of *Active and Quasi-Optical Arrays for Solid-State Power Combining* (New York: Wiley, 1997). Her research interests include microwave active antennas, smart antennas, high-efficiency microwave circuits, quasioptical techniques, RF photonics, receivers for radioastronomy, and front ends for communication systems.

Dr. Popovic received the 1993 IEEE MTT Microwave Prize, 1993 URSI Young Scientist and NSF Presidential Faculty Fellow awards, and 1996 URSI Issac Koga Gold Medal. In 1997, she was chosen Professor of the Year by Eta Kappa Nu students. In 2000, she received a Humboldt Research Award for Senior U.S. Scientists from the German Alexander von Humboldt Foundation.